IOP Publishing | Institute of Physics and Engineering in Medicine Physics in Medicine & Biology

Phys. Med. Biol. **61** (2016) 8214–8231 doi:10.1088/0031-9155/61/23/8214

egs_brachy: a versatile and fast Monte Carlo code for brachytherapy

Marc J P Chamberland, Randle E P Taylor, D W O Rogers and Rowan M Thomson

Carleton Laboratory for Radiotherapy Physics, Department of Physics, Carleton University, Ottawa, Ontario, K1S 5B6, Canada

E-mail: rthomson@physics.carleton.ca

Received 18 August 2016
Accepted for publication 4 October 2016
Published 2 November 2016

Abstract

egs_brachy is a versatile and fast Monte Carlo (MC) code for brachytherapy applications. It is based on the EGSnrc code system, enabling simulation of photons and electrons. Complex geometries are modelled using the EGSnrc C++ class library and egs_brachy includes a library of geometry models for many brachytherapy sources, in addition to eye plaques and applicators. Several simulation efficiency enhancing features are implemented in the code. egs_brachy is benchmarked by comparing TG-43 source parameters of three source models to previously published values. 3D dose distributions calculated with egs_brachy are also compared to ones obtained with the BrachyDose code. Well-defined simulations are used to characterize the effectiveness of many efficiency improving techniques, both as an indication of the usefulness of each technique and to find optimal strategies. Efficiencies and calculation times are characterized through single source simulations and simulations of idealized and typical treatments using various efficiency improving techniques. In general, egs_brachy shows agreement within uncertainties with previously published TG-43 source parameter values. 3D dose distributions from egs_brachy and BrachyDose agree at the sub-percent level. Efficiencies vary with radionuclide and source type, number of sources, phantom media, and voxel size. The combined effects of efficiency-improving techniques in egs_brachy lead to short calculation times: simulations approximating prostate and breast permanent implant (both with $(2\,\text{mm})^3$ voxels) and eye plaque (with $(1\,\text{mm})^3$ voxels) treatments take between 13 and 39 s, on a single 2.5 GHz Intel Xeon E5-2680 v3 processor core, to achieve 2% average statistical uncertainty on doses within the PTV. egs_brachy will be released as free and open source software to the research community.

Keywords: brachytherapy, dosimetry, Monte Carlo, EGSnrc, egs_brachy, variance reduction techniques

(Some figures may appear in colour only in the online journal)

1. Introduction

Brachytherapy plays an important role in the treatment of various cancers, including breast, prostate, gynecological, and ocular cancers (Thomadsen *et al* 2008). In cancer centers, doses for brachytherapy treatments are computed using the formalism described by Task Group 43 (TG-43) of the American Association of Physicists in Medicine (AAPM) (Rivard *et al* 2004): doses are calculated as the superposition of dose distributions for individual sources which were pre-calculated assuming a water environment. The speed of TG-43 dose calculations comes at the expense of accuracy. These simplified calculations ignore factors which can significantly impact dose distributions, such as tissue inhomogeneities, the presence of nearby objects with elemental compositions different from water, and the attenuation of photons by the seeds themselves (see Beaulieu *et al* (2012) and references therein).

With the goal of reducing differences between calculated and delivered doses, momentum is growing for adoption of model-based dose calculation algorithms (MBDCAs) in brachytherapy. A number of codes have been developed to carry out advanced model-based dose calculations for brachytherapy; see the report of AAPM Task Group 186 (Beaulieu *et al* 2012) and references therein, Chibani and Williamson (2005), Taylor *et al* (2007), Thomson *et al* (2010), Afsharpour *et al* (2012), Chibani and Ma (2014) and Bonenfant *et al* (2015). Two MBDCA options are available in commercial treatment planning systems: Acuros (a grid-based Boltzmann equation solver) in Brachy Vision[1] and ACE (a collapsed cone superposition/convolution method) in Oncentra Brachy[2] (Papagiannis *et al* 2014). Although the Monte Carlo (MC) technique has long been recognized a highly accurate computational dosimetry method, its routine clinical use has been limited due to long calculation times. Further, many brachytherapy-specific MC codes are not widely available.

BrachyDose (Taylor *et al* 2007, Thomson *et al* 2010), an EGSnrc (Kawrakow *et al* 2011) user code which uses the multi-geometry package by (Yegin 2003), was developed to address this need. However, in the years since the development of BrachyDose, the highly versatile, open source, and actively-maintained EGSnrc C++ class library (Kawrakow *et al* 2009) (called egs++) was released. This motivated the development of egs_brachy, a modern EGSnrc application using egs++ for modelling geometries and particle sources, designed specifically for brachytherapy applications. In addition, egs_brachy also led to several enhancements to the general-purpose egs++ library in the form of new geometry and shape classes.

Figure 1 provides an overview of the egs_brachy application. Like most other distributed EGSnrc user codes, egs_brachy relies on a text-based input file to define all aspects of the simulation. egs_brachy can be used for a comprehensive set of brachytherapy simulations, such as dose calculations, generation of phase-space data and calculation of particle spectra. egs_brachy also incorporates features to enhance simulation efficiency, including efficient radiation transport and geometry modelling, calculation of collision kerma using the track-length estimator, phase-space sources, particle recycling, and variance reduction techniques for electronic brachytherapy. A library of pre-defined source, applicator, and phantom geometries is distributed with the system.

[1] Varian Medical Systems, Palo Alto, CA.
[2] Elekta, Veenendaal, Netherlands.

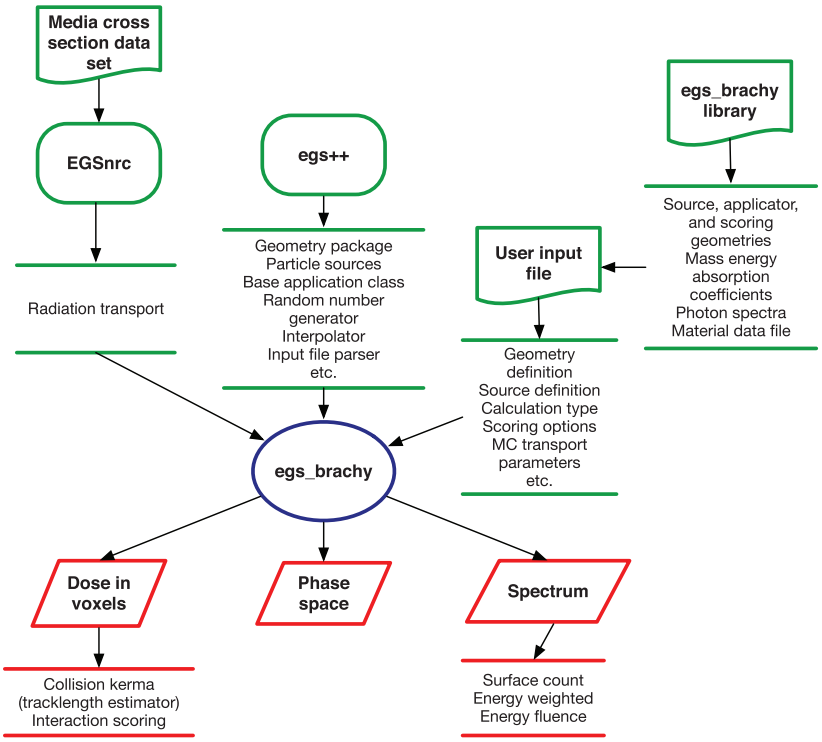

Figure 1. Schematic diagram for egs_brachy.

The current work provides benchmarks of the code against other published data, and assesses the efficiency gains from various techniques implemented in the code. egs_brachy is benchmarked by reproducing previously published TG-43 source parameters for three brachytherapy source models and comparing 3-D dose distributions calculated using egs_brachy and BrachyDose. The various egs_brachy features to enhance simulation efficiency are characterized through example simulations and calculation times for realistic clinical scenarios are presented.

2. Methods

2.1. The egs_brachy application

As egs_brachy is an EGSnrc application, both photon and electron transport may be modelled. This permits simulation of electronic sources (for example, miniature x-ray tubes and beta-emitting eye plaques) in addition to photon (radionuclide) brachytherapy sources. Although egs_brachy is capable of modelling electron transport, the low energy of photons from brachytherapy sources means that dose is well approximated by collision kerma for most situations of interest. Hence, generally only the simulation of photon transport is necessary and electron transport is turned off by appropriate choice of the electron cutoff energy. Complex geometries can be modelled using the built-in elementary and composite geometries of egs++. A rectilinear phantom may be defined by a CT dataset using the egsphant file format also used with the EGSnrc user code DOSXYZnrc.

The code scores dose or collision kerma in rectilinear voxels or in spherical or cylindrical shells[3]. A fast envelope geometry class, **`EGS_AutoEnvelope`**, is used to inscribe one or more copies of source geometries inside a phantom. Voxels containing part of a source geometry are automatically identified during the initialization of the simulation geometry. During particle transport, if a voxel contains no source, then there is no check of the boundaries of source geometries. The distribution of radioactivity within a source is defined by sampling random points from a user-specified shape. Two new egs++ shape classes, **`EGS_ConicalShellStackShape`** and **`EGS_SphericalShellShape`**, sample random points within conical and spherical shells, respectively. The additions to egs++ will be available as part of the next major release of the EGSnrc distribution.

egs_brachy has three run modes which permit different types of simulations: *normal*, *superposition*, and *volume correction only*. The default run mode for simulations is *normal*. The *superposition* run mode may be used with more than one brachytherapy source, but only one source is 'active' at a time. This run mode is suitable for simulating HDR treatments (in which a single source steps through dwell positions) and for removing interseed effects. The *volume correction only* run mode calculates volume corrections needed when objects occupy part of a scoring voxel, outputs the results, and then quits; no radiation transport is done.

At low photon energies, dose can be approximated as collision kerma, which egs_brachy scores using a tracklength estimator (see Williamson (1987)). For consistency, this requires use of mass energy absorption coefficients for each material calculated with the same cross sections as used for the simulation of radiation transport (for example, using the EGSnrc application 'g'). egs_brachy can also score dose using interaction scoring which is much less efficient but can be used to account for electron transport where charged particle equilibrium does not exist.

Whether dose is approximated as collision kerma or absorbed dose is calculated, statistical uncertainties on dose are evaluated using history-by-history statistics (Walters *et al* 2002). Dose in voxel j is output normalized as dose per effective starting particle, N_{eff} (table 1). For simulations in which starting particles are initiated within the radioactivity distribution within the source (herein referred to as '*ab initio*'), N_{eff} is just the number of histories, N_h. When a phase-space source or the particle recycling feature are used, N_{eff} is the number of independent histories that would have to be simulated in an *ab initio* simulation to obtain the same number of scoring particles.

At the request of the user, dose is scored separately for primary, single-scattered, and multiple-scattered particles according to the Primary Scatter Separated (PSS) dose formalism (Russell *et al* 2005). egs_brachy can tabulate phase-space data on the surface of a source for all particles emitted from the source. Three spectrum scoring options are available in egs_brachy: the first is an absolute count of the particles escaping a source; the second is an energy-weighted spectrum of particles scored on the surface of a source; and the third is an energy fluence spectrum scored in a voxel.

2.2. Features to enhance simulation efficiency

In addition to the tracklength estimator to score collision kerma and the **`EGS_AutoEnvelope`** geometry class mentioned above, other features to enhance simulation efficiency are discussed in the current section. The metric to quantify simulation efficiency is

$$\epsilon = \frac{1}{s^2 t}, \tag{1}$$

[3] Using an addition to the egs++ geometry library developed in conjunction with egs_brachy.

Table 1. Effective number of histories, N_{eff}, for different simulations where N_h is the number of initial histories.

Simulation	Description	Effective number of histories, N_{eff}
(1) *Ab initio* (default)	All particles initialized within each source	N_h
(2) *Ab initio* with recycling	Particles initialized within one source; particles escaping that source are recycled n_r times at each of the n_s source locations	$N_h\, n_s\, n_r$
(3) Phase-space source	Initialize $N_1 \leqslant N_{\text{emit}}$ particles from a file containing data for N_{emit} particles from simulation of N_h (initial) histories	$\frac{N_1 N_h}{N_{\text{emit}}}$
(4) Phase-space source and recycling	Phase-space source as in (3) with recycling as in (2)	$\frac{N_1 n_s n_r N_h}{N_{\text{emit}}}$

where t is the total CPU simulation time for transport and scoring needed to compute a chosen quantity with uncertainty s, but t does not include the time to initialize the simulation and the geometry, output the results, etc.

For simulations of $n_s > 1$ sources of the same model with the *normal* run mode, it is not necessary to repeat the simulation of photons within a source for every history. With the particle recycling feature, the first source in the simulation acts as a particle generator. Particles initiated in this source are tracked until they are either absorbed within it or they escape the source encapsulation. An escaping particle is translated and initiated for each source at the same relative position as it escaped the first source. The recycled particles can optionally be randomly rotated about the source axis before being reinitiated at each source location. Each generated particle may be recycled more than once (n_r times) at each source location; in this case, the rotation is not optional and particles are rotated before each reuse. The computation of statistical uncertainties accounts for correlations between recycled particles: the history counter is incremented by one for each set $n_s n_r$ of recycled particles to preserve the history-by-history statistics (table 1).

A phase-space source can be used instead of initiating particles within a source geometry. A user-specified number of particles, N_1, is initiated on the surface of sources from the phase-space data. If the user wishes to simulate more starting particles than there are data for in the phase space (i.e., $N_1 > N_{\text{emit}}$), it is recommended that particle recycling be used in conjunction with the phase-space source to account for correlations between particles from the same primary history (table 1).

The standard EGSnrc variance reduction techniques of bremsstrahlung cross section enhancement (BCSE), uniform bremsstrahlung splitting (UBS), Russian roulette, and range rejection are available to enhance simulation efficiency of electron transport. The BCSE feature allows the user to specify a factor f_{enh} by which to scale up the bremsstrahlung production cross section in the target material. With UBS, each generated bremsstrahlung photon is split into N_{split} photons (with N_{split} specified by the user). If BCSE or UBS are used, then Russian roulette is automatically activated and secondary charged particles produced have a survival probability of $1/(f_{\text{enh}} N_{\text{split}})$. Range rejection of charged particles is enabled by default in the phantom voxels.

2.3. Simulations

Simulations with egs_brachy are carried out for benchmarking, characterization of simulation efficiencies, and determination of calculation times with clinical configurations (table 2).

Table 2. Description of configurations for calculations carried out for benchmarking (a, b, j, m), characterization of simulation efficiencies (c → o), and determination of calculation times (p → r).'Voxel size' applies to the voxels in the scoring region only. Most phantoms have dimensions that extend beyond the scoring region. Source models are TheraSeed 200 (^{103}Pd), OncoSeed 6711 (^{125}I), and microSelectron v2 HDR (^{192}Ir).

Simulation	'ID'	Phantom	Source (#)	Scoring region (cm^3)	Voxel size
TG-43	'a'	Water cylinder, 30 cm length, 15 cm radius	^{103}Pd (1) or ^{125}I (1)	Cylindrical shells	Width and thickness: 0.1 mm ($r \leqslant 1$ cm), 0.5 mm ($1 < r \leqslant 5$ cm), 1 mm ($5 < r \leqslant 10$ cm)
	'b'	Water cylinder, 80 cm length, 40 cm radius	^{192}Ir (1)	Cylindrical shells	Same as a, with 2 mm ($10 < r \leqslant 20$ cm)
Single source	'c'	Water (30 cm)^3	^{103}Pd, ^{125}I, or x-ray tube (1)	$2 \times 2 \times 2$	(1 mm)^3
	'd'	Water (30 cm)^3	^{192}Ir (1)	$4 \times 4 \times 4$	(1 mm)^3
	'e'	Water (4.80 cm)^3	^{103}Pd (1)	$2.45 \times 2.45 \times 2.45$	(0.49 mm)^3
	'f'	Water (10.0 cm)^3	^{125}I (1)	$5.35 \times 5.35 \times 5.35$	(1.07 mm)^3
	'g'	Water (53.1 cm)^3	^{192}Ir (1)	$27.7 \times 27.7 \times 27.7$	(5.54 mm)^3
Prostate	'h'	Prostate[a] (30 cm)^3	^{125}I (100)	$3.4 \times 2.8 \times 3.8$	(1 mm)^3
	'i'	Prostate[a] (30 cm)^3	^{125}I (100)	$3.4 \times 2.8 \times 3.8$	(2 mm)^3
	'j'	Water (30 cm)^3	^{125}I (100)	$3.4 \times 2.8 \times 3.8$	(2 mm)^3
Eye	'k'	Eye[b] (30 cm)^3	^{125}I (13)	$3 \times 3 \times 3$	(0.5 mm)^3
	'l'	Water (30 cm)^3	^{125}I (13)	$3 \times 3 \times 3$	(0.5 mm)^3
	'm'	Water (30 cm)^3	^{125}I (13)	$3 \times 3 \times 3$	(1 mm)^3
Breast LDR and HDR	'n'	Breast[c] 3868 cm^3	^{103}Pd (64) or ^{192}Ir (30[g])	$4 \times 4 \times 4$	(0.5 mm)^3
	'o'	Water 3868 cm^3	^{103}Pd (64) or ^{192}Ir (30[g])	$4 \times 4 \times 4$	(2 mm)^3
Clinical	'p'	Breast[d] 4910 cm^3	^{103}Pd (49)	$19 \times 19 \times 13.6$	(2 mm)^3
	'q'	Breast[e] 13548 cm^3	^{192}Ir (79[g])	$33.6 \times 33.6 \times 12$	$2 \times 2 \times 3$ mm^3
	'r'	Prostate[f] 2482 cm^3	^{125}I (67)	$15.6 \times 15.6 \times 10.2$	(2 mm)^3

[a] Homogeneous, density 1.04 g cm^{-3}, with elemental composition from Woodard and White (1986).
[b] Egsphant model of the eye from Lesperance *et al* (2014); includes non-water media for ocular structures and surrounding tissues.
[c] Egsphant model of the breast from Sutherland *et al* (2011); includes gland and adipose tissues.
[d] Virtual patient phantom from CT data, with tissue assignment scheme (TAS) from Miksys *et al* (2016a).
[e] Virtual patient phantom from CT data from Peppa *et al* (2016), with TAS from Miksys *et al* (2016a).
[f] Virtual patient phantom from CT data, with TAS from Miksys *et al* (2016a).
[g] Number of dwell positions.

In all calculations, the photon cutoff energy is set to 1 keV and electron transport is generally not modelled. Rayleigh scattering, bound Compton scattering, photoelectric absorption, and fluorescent emission of characteristic x-rays are all modelled. Atomic transitions available in the Livermore Evaluated Atomic Data Library (EADL) (Perkins *et al* 1991) are modelled explicitly[4]. Photon cross sections are from the XCOM database (Berger and Hubbell 1987). Mass-energy absorption coefficients are calculated using the EGSnrc user code *g*. Photon

[4] But the M and N shells were treated in an average way for the comparisons reported here.

spectra from the NNDC (Brookhaven National Laboratory, National Nuclear Data Center) (^{103}Pd and ^{192}Ir) are used to sample initial photon energies and probabilities. For ^{125}I, the photon spectrum from the NCRP Report 58 (1985) is used since Rodriguez and Rogers (2013) demonstrated that using the NCRP spectrum leads to much better agreement with calculated spectra and is consistent with the spectrum recommended by the BIPM for use by primary standards labs (BIPM 2011). Calculations are carried out on a single 2.5 GHz Intel Xeon E5-2680 v3 processor core, with egs_brachy compiled using gcc version 4.1.2 20080704. For calculation of the efficiency, ϵ, (equation (1)) the uncertainty s^2 is taken as the quadrature sum of percent statistical uncertainties on all doses to scoring voxels in the region of interest, not only those with dose above some threshold.

2.3.1. Benchmarking. egs_brachy is benchmarked against BrachyDose, which has been extensively validated in the past (Taylor *et al* 2007, Taylor and Rogers 2008a, 2008b, Thomson *et al* 2008, Rivard *et al* 2011, Ballester *et al* 2015). TG-43 source parameters are calculated for three source models using an approach similar to that used by Taylor and Rogers (2008a, 2008b) using BrachyDose. Configurations 'a' and 'b' are used for the low-energy seeds (^{103}Pd and ^{125}I) and the high-energy source (^{192}Ir), respectively. Extracted TG-43 parameters are compared to those previously published for BrachyDose as well as to other published values.

In addition, dose distributions for configurations 'j' and 'm' are calculated with egs_brachy and BrachyDose. Configuration 'j' approximates a prostate LDR treatment with 100 ^{125}I seeds arranged in a $5 \times 4 \times 5$ grid. Nominal source center-to-center distances of 7 mm in the x and y-directions and 8 mm in the z-direction are perturbed randomly by up to 0.5 mm. Configuration 'm' includes a COMS 16 mm plaque (Thomson *et al* 2008) containing 13 ^{125}I seeds; BrachyDose dose distributions were previously shown to agree within statistical uncertainties with published MCNP5 results (Rivard *et al* 2011). Comparisons of the 3D dose distributions for configurations 'j' and 'm' are done with the approach of Kawrakow and Fippel (2000): a function which separates systematic uncertainties from expected statistical uncertainties is fit to the distribution of voxel-by-voxel dose differences (in units of the combined uncertainty on doses in each voxel). The function is the probability distribution $f(x)$ to find a voxel with dose difference x and is given by:

$$f(x) = \frac{1}{\sqrt{2\pi}}\left[\alpha_1 \exp\left(-\frac{(x-\Delta_1)^2}{2}\right) + \alpha_2 \exp\left(-\frac{(x-\Delta_2)^2}{2}\right) + (1-\alpha_1-\alpha_2)\exp\left(-\frac{x^2}{2}\right)\right], \quad (2)$$

where α_1 and α_2 are the fraction of voxels that have a systematic difference of Δ_1 and Δ_2, respectively.

2.3.2. Characterization of simulation efficiency.

Single radionuclide source. For each source model studied (see table 2), a single source is modelled at the center of configurations 'c' (^{103}Pd and ^{125}I) and 'd' (^{192}Ir). A second set of simulations is performed with the source at the center of configurations 'e', 'f', and 'g', with phantom dimensions motivated by consideration of energy deposition about a single source. The dimensions were determined using results for dose scored in concentric spherical shells

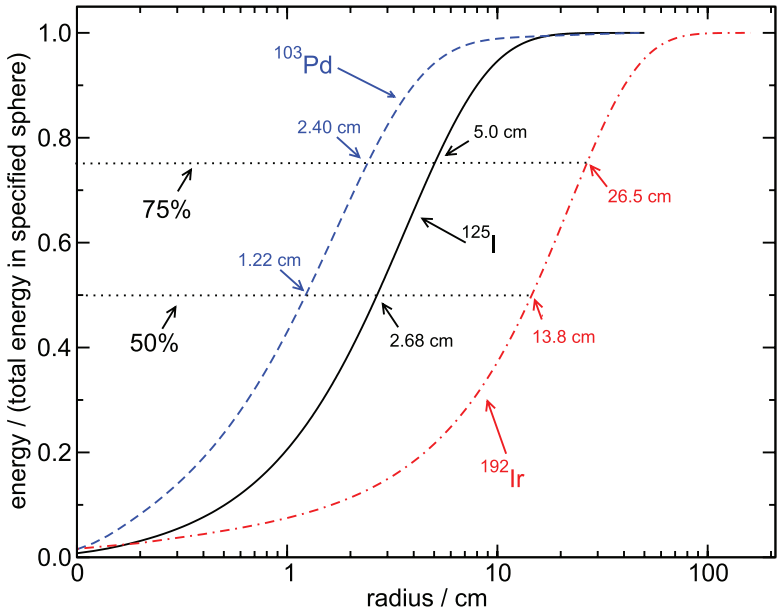

Figure 2. Fraction of energy deposited within water sphere of given radius versus radius for ^{125}I (OncoSeed 6711), ^{103}Pd (TheraSeed 200), and ^{192}Ir (microSelectron v2 HDR) sources. The single source was simulated at the center of a water sphere of radius 50 cm (^{103}Pd and ^{125}I) and 160 cm (^{192}Ir).

about a single source at the center of a large water sphere (figure 2). The rectilinear phantoms have side length $2R_{75}$, where R_{75} is the radius of the sphere within which 75% of the energy is deposited. Similarly, the scoring regions have side length $2R_{50}$, where R_{50} is the radius of the 50% energy deposition sphere.

Prostate permanent implant. The prostate configuration used for benchmarking ('j', with 100 ^{125}I seeds) is used again for characterization of efficiency gains. In addition, configurations 'h' and 'i' are also used, with the same arrangement of ^{125}I seeds.

Eye plaque. Simulations are performed with configurations 'k', 'l', and 'm', and include a COMS 16 mm plaque containing 13 ^{125}I seeds (Thomson *et al* 2008). For calculation of efficiency, only the voxels containing tumor tissue in the egsphant ('k') and the corresponding voxels in the water phantoms ('l', 'm') are considered. The size of the target volume is 0.2995 cm^3 (2396 voxels) and 0.414 cm^3 (414 voxels) for 'l' and 'm', respectively.

Breast permanent implant. Simulations are performed with configurations 'n' and 'o', with 64 ^{103}Pd seeds in a cubic formation about the center of the phantom, with central x, y, and z coordinates of ± 1.55 cm or ± 0.55 cm.

HDR breast. Configurations 'n' and 'o' are used again, with an ^{192}Ir source modelled at 30 dwell positions ($x, y = 0, \pm 1.0$; $z = 0, \pm 0.67, \pm 1.33$; all cm).

Electronic brachytherapy. A miniature electronic brachytherapy source is modelled at the center of configuration 'c'. The model of the source is inspired by the Xoft Axxent source

(Taylor *et al* 2006). Using monoenergetic 50 keV electrons as starting particles, the following simulations are performed: *ab initio* (electron transport within the source only and photon transport only elsewhere in the phantom) and also using BCSE and UBS with Russian roulette employing the optimum parameters reported by Ali and Rogers (2007) for the $(1\,\text{mm})^3$ grid of voxels they considered: $f_{\text{enh}} = 500$ and $N_{\text{split}} = 100$. In addition, the phase space of photons emitted from the source is scored and used to initiate a simulation.

2.3.3. Calculation times for clinical configurations. Configurations 'p', 'q', and 'r' are used to illustrate realistic egs_brachy timing in a clinical setting to reach a given metric (2% average statistical uncertainty on doses to the PTV; 5% on doses to the organs at risk). Configuration 'p' corresponds to a breast LDR treatment; 'q' corresponds to a breast HDR treatment; and 'r' corresponds to a prostate LDR treatment. Only voxels with doses greater than 25% of the prescription dose are considered in the calculation of the uncertainties in the volumes of interest.

3. Results and discussion

3.1. Benchmarking

A summary of benchmarking results is shown in figure 3 which displays radial dose functions and anisotropy functions at 1 cm, as calculated by egs_brachy and BrachyDose. Dose-rate constants are shown in table 3. Agreement within uncertainties between the two codes is found for all TG-43 source parameters, as well as agreement within uncertainties with measured dose rate constants.

The distributions of dose differences between egs_brachy and BrachyDose 3D dose distributions for the prostate ('j') and eye plaque ('m') configurations are shown in figure 4. Equation (2) is fit to each distribution and the parameters α_1, Δ_1, α_2, and Δ_2 are extracted, if applicable. For 99% of the voxels in the prostate case, the systematic difference is a small fraction (0.03) of the average combined uncertainty of the two dose distributions (0.6%). For 14% of the voxels in the eye plaque case, the systematic difference is 0.77 of the average combined uncertainty (0.6%), which corresponds to a systematic difference of 0.46%. For both simulation geometries, the doses to the remaining voxels agree between the two codes within statistical uncertainties. The systematic differences observed are either much smaller than other typical Monte Carlo systematic uncertainties (which add up in quadrature to 1.5–2.5%) (Rivard *et al* 2004, Rodriguez and Rogers 2014) or they affect a small fraction of voxels (14%). Note that the results from the fit are sensitive to the width of the bins used. For example, using bins of width 0.2 (instead of 0.1) yields $\alpha_1 = 0.83$, $\Delta_1 = 0.08$, and $\alpha_2 = 0$ for 'j'. However, this effect does not change the interpretation of the results.

3.2. Characterization of simulation efficiency

3.2.1. Single radionuclide source. Efficiencies for *ab initio* and phase-space source simulations of single ^{125}I, ^{103}Pd, and ^{192}Ir sources at the center of a water phantom vary with radionuclide and phantom (table 4). For the more clinically-relevant $(30\,\text{cm})^3$ phantom with $(1\,\text{mm})^3$ voxels ('c', 'd'), simulations with a phase-space source have efficiencies enhanced by a factor of 1.12 (^{192}Ir) to 2.08 (^{103}Pd) over *ab initio* simulations. Thus, an *ab initio* simulation takes longer than one employing a phase-space source. For example, for ^{103}Pd, a 1% square-root quadrature sum uncertainty for the $(2\,\text{cm})^3$ grid of $(1\,\text{mm})^3$ voxels will be achieved in 89 s for phase-space source simulations and 184 s for *ab initio* simulations. For any phantom considered, the most substantial efficiency gains from using a phase-space source are

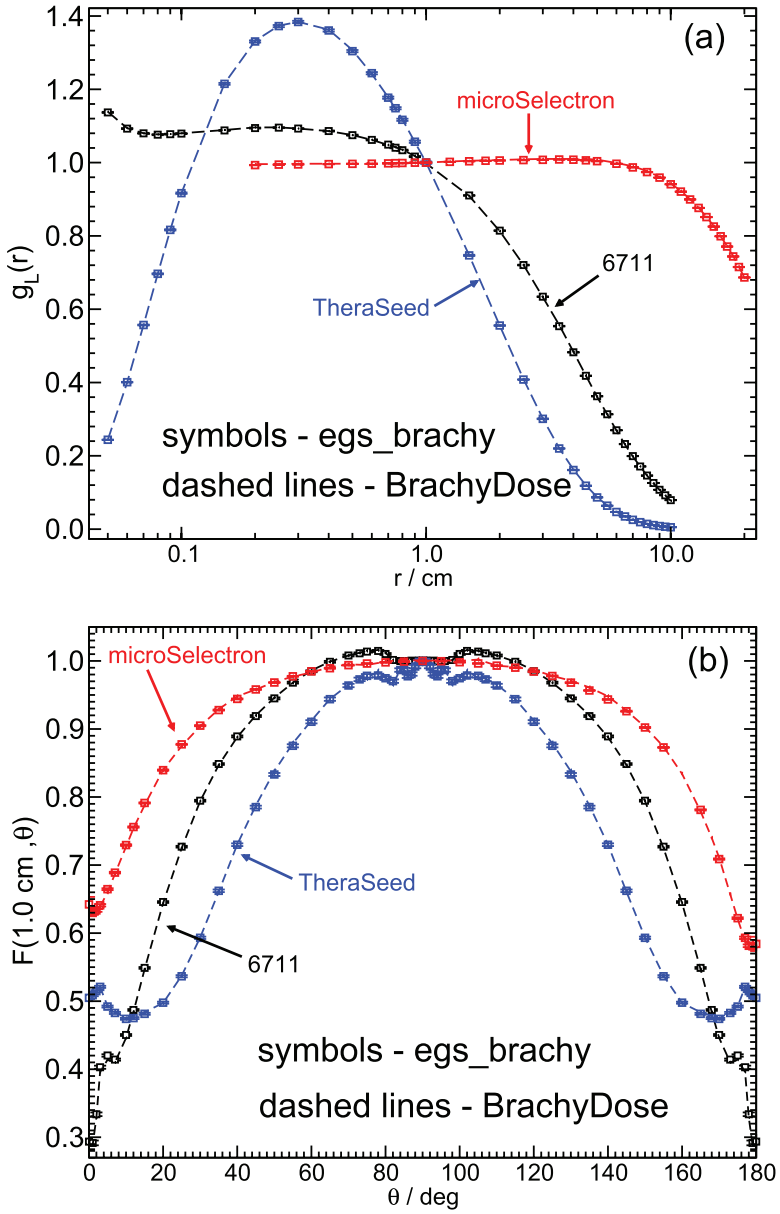

Figure 3. TG-43 source parameters comparison between egs_brachy (symbols) and BrachyDose (dashed lines) for three source models: Amersham OncoSeed 6711, Theragenics TheraSeed 200, and Nucletron microSelectron v2 HDR. (a) Radial dose function. (b) Anisotropy function at 1 cm from the source. More results for all source models referred to in this study are also available on an updated version of the CLRP TG-43 web database (https://physics.carleton.ca/clrp/egs_brachy/seed_database_v2).

achieved for the lower-energy sources for which a significant fraction of photons are absorbed within the source. For a given radionuclide, there are no significant differences in efficiencies between different source models (results not shown). Efficiency improvements are less dramatic between the three radionuclides for the phantoms of varying sizes ('e', 'f', 'g').

Table 3. Calculated ('egs_brachy' and 'BrachyDose') and measured ('Experimental') dose-rate constant values. Values from egs_brachy and BrachyDose have statistical component of uncertainties of 0.3% or less.

	Dose-rate constant Λ (cGy h^{-1} U^{-1})		
Source	egs_brachy	BrachyDose	Experimental
^{103}Pd TheraSeed, 200 (Theragenics)	0.684 ± 1.5%	0.685 ± 1.5%[a]	0.68 ± 7.4%[c]
^{125}I OncoSeed, 6711 (Amersham)	0.931 ± 1.5%	0.928 ± 1.5%[a]	0.92 ± 6.0%[d]
^{192}Ir microSelectron v2, HDR (Nucletron)	1.108 ± 1.5%	1.109 ± 1.5%[b]	N/A

[a] Rodriguez and Rogers (2014). [b] Taylor and Rogers (2008b). [c] Nath *et al* (2000). [d] Kennedy *et al* (2010).

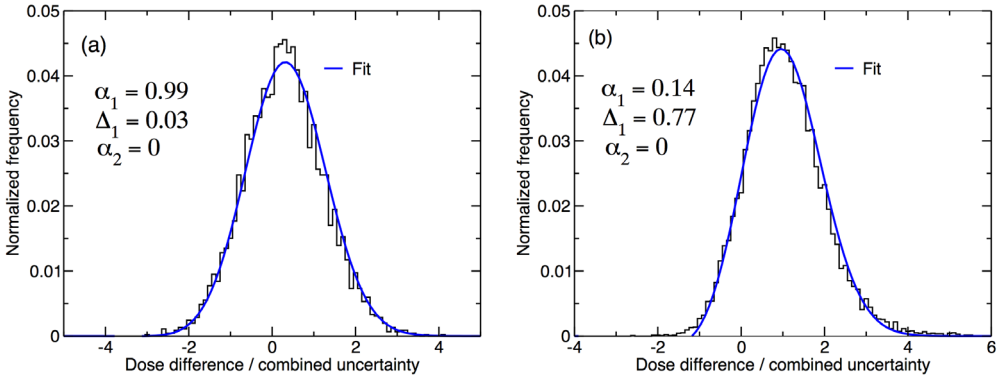

Figure 4. The distribution of dose differences (in units of the combined uncertainty with a bin width of 0.1) between egs_brachy and BrachyDose 3D dose distributions for (a) the prostate and (b) the eye plaque configurations. The fit to equation (2) is shown along with the fitted parameters.

Table 4. Single source simulation efficiencies (all with tracklength scoring) for ^{125}I, ^{103}Pd, and ^{192}Ir sources at the center of water phantoms. Results are provided for both *ab initio* simulations and for simulations employing a phase-space source. s^2 is the quadrature sum of percent statistical uncertainties on doses to scoring voxels. The time in seconds to achieve $s = 1\%$ is $1/\epsilon$. Efficiencies of phase-space source simulations relative to *ab initio* simulations are indicated in parentheses.

	$1000 \times \epsilon = 1000 \times 1/s^2 t$ (s^{-1})			
	(30 cm)^3 phantom[a]		Varying phantom size[b]	
Source	*Ab initio*	Phase space	*Ab initio*	Phase space
^{103}Pd TheraSeed, 200 (Theragenics)	5.42	11.3 (2.08)	0.503	0.751 (1.49)
^{125}I OncoSeed, 6711 (Amersham)	7.97	12.2 (1.53)	0.510	0.688 (1.35)
^{192}Ir microSelectron v2, HDR (Nucletron)	1.36	1.52 (1.12)	0.536	0.576 (1.07)

[a] Configurations 'c' (^{103}Pd and ^{125}I) and 'd' (^{192}Ir).
[b] Configurations 'e', 'f', and 'g' (^{103}Pd, ^{125}I, and ^{192}Ir, respectively).

Table 5. Variation in prostate simulation times (configurations 'h' and 'i') with the number of ^{125}I seeds and voxel sizes (with tracklength scoring). CPU times for radiation transport (with or without the use of the **EGS_AutoEnvelope** geometry class) and the square root of the quadrature sum of percent statistical uncertainties on doses to voxels within the PTV are given for simulations of 4×10^7 histories for three $(30\,\text{cm})^3$ water phantoms with a central $36.2\,\text{cm}^3$ PTV (containing all seeds) with differing voxel grids. The CPU time without **EGS_AutoEnvelope** relative to the CPU time with **EGS_AutoEnvelope** is shown in parentheses. The times and uncertainties shown illustrate trends; these specific values depend on source positions.

		Time for 4×10^7 hist. (s)		
Voxel size	Number of seeds	With autoenvelope	Without autoenvelope	Uncertainty in PTV (%)
$36.2\,\text{cm}^3$	100	265	227 (0.9)	0.030
	1	111	104 (0.9)	0.020
$(2\,\text{mm})^3$	100	194	652 (3.4)	0.65
	10	195	240 (1.2)	0.74
	1	176	166 (0.9)	0.78
$(1\,\text{mm})^3$	100	237	1083 (4.6)	1.3
	10	251	345 (1.4)	1.5
	1	245	229 (0.9)	1.6

3.2.2. Multiple sources. Simulation times generally increase with the number of sources simulated and with smaller voxel sizes. Table 5 reports simulation times for different numbers of ^{125}I seeds in configurations 'h' and 'i', in addition to a configuration with a single voxel ($36.2\,\text{cm}^3$) spanning the PTV. When not using **EGS_AutoEnvelope**, simulation times range from 104 s (single seed in a single $36.2\,\text{cm}^3$ voxel) to 1083 s (100 seeds in a PTV filled with $(1\,\text{mm})^3$ voxels) and increases with the number of voxels as voxel size decreases. With **EGS_AutoEnvelope**, simulation times are up to 4.6 times shorter (100 seeds in a PTV filled with $(1\,\text{mm})^3$ voxels). The time to identify phantom voxels containing source geometries varies from 0.01 s (single seed) to 1 s (100 seeds in $(1\,\text{mm})^3$ voxels), which is negligible compared to the CPU time spent on radiation transport. The efficiency gain of using **EGS_AutoEnvelope** increases with the number of seeds and is larger for smaller voxels (for which a larger number of voxels do not contain source geometries). Using **EGS_AutoEnvelope** provides the advantage of calculation times that are effectively independent of the number of seeds modelled. For a single source or a single voxel simulation, using **EGS_AutoEnvelope** results in slightly slower calculations, but those configurations are not typically relevant in a clinical setting.

Table 6 presents efficiencies for the various example simulation geometries with ^{125}I, ^{103}Pd, or ^{192}Ir sources. Tracklength rather than interaction scoring of collision kerma results in efficiency gains of factors of 10 to more than 300. Efficiency gains from the phase-space source and recycling features of egs_brachy are more modest than those for going from interaction scoring to tracklength scoring but are still considerable in achieving clinically-reasonable calculation times. Efficiency gains vary with radionuclide, source model, number of sources, simulation type, phantom media and extent, and voxel size.

For prostate simulations, simulations in prostate medium ('i') or in water ('j') with the same $(2\,\text{mm})^3$ voxel grid have comparable efficiencies (table 6). Efficiencies are expected to vary somewhat with phantom medium due to voxel-by-voxel cross section variations affecting radiation transport and energy deposition. Hence efficiencies are not identical for prostate

Table 6. Efficiencies for simulations of prostate, eye, and breast brachytherapy with configurations described in table 2. Collision kerma is scored using tracklength scoring in all cases, except for the column labeled *Interaction*. For *Recycling*, particles are initiated within the first seed and emitted particles are reinitiated once at other seed locations, without rotation of the recycled particles around the source. The phase space is not recycled. The efficiency relative to that for the *ab initio* simulation is indicated in parentheses. The time in seconds to achieve $s = 1\%$ is $1/\epsilon$. Times for simulations employing a phase-space source do not include the time to generate the phase-space data.

			$1000 \times \epsilon = 1000 \times 1/s^2t$ (s^{-1})			
Simulation	Radio-nuclide	Configuration	*Ab initio*	Interaction, *ab initio*	Recycling	Phase space
Prostate	^{125}I	'h'	2.38	0.055 (0.023)	4.12 (1.73)	4.18 (1.76)
		'i'	12.9	0.577 (0.045)	23.8 (1.85)	26.1 (2.02)
		'j'	13.0	0.562 (0.043)	24.9 (1.91)	27.3 (2.09)
Eye	^{125}I	'k'	2.43	0.033 (0.013)	3.48 (1.43)	3.73 (1.53)
		'l'	3.51	0.038 (0.011)	5.52 (1.57)	5.61 (1.60)
		'm'	16.0	0.349 (0.022)	26.9 (1.69)	28.2 (1.77)
Breast LDR	^{103}Pd	'n'	0.125	0.002 (0.015)	0.18 (1.42)	0.16 (1.31)
		'o'	4.29	0.404 (0.094)	10.4 (2.43)	9.35 (2.18)
Breast HDR	^{192}Ir	'n'	0.0877	0.0003 (0.0032)	[a]	0.11 (1.20)
		'o'	1.70	0.023 (0.013)	[a]	1.83 (1.08)

[a] Results with particle recycling are not reported for the HDR treatment as particle recycling is not compatible with the *superposition* run mode used for these simulations.

simulations in water or non-water media with the same voxel grid. However, the comparable efficiencies in water and non-water media in table 6 are in contrast with the results of Afsharpour *et al* (2012) who report time differences of factors of two or more for water versus non-water simulations using their Geant4-based code ALGEBRA for prostate and breast LDR simulations. This is due to the fact that Geant4 (ALGEBRA) does not look up cross sections when crossing voxel boundaries for the homogeneous water calculations, but it does for the heterogeneous media calculations. In contrast, EGSnrc (egs_brachy) looks up cross sections for each voxel no matter the simulation geometry and hence calculation time does not change substantially.

Simulation efficiency is enhanced over *ab initio* simulations by factors of 1.08–2.18 using phase-space sources and by factors of 1.42–2.43 using particle recycling without rotation of the particles around the long axis of the source. In many cases, efficiencies for simulations with recycling are comparable to those using a phase-space source. Hence, recycling is effective at improving simulation efficiency without the need to generate and store large phase-space files since, for many seeds, the overall time spent simulating transport inside seeds is relatively small when recycling. In general, rotating recycled particles does not significantly improve efficiency over recycling particles without rotation. Recycling particles more than once at each source location does not lead to further efficiency gains.

The combined effects of the different egs_brachy features to enhance simulation efficiencies result in short simulation times which can be deduced from the efficiencies presented in table 6. For more accurate estimates of egs_brachy timing, the simulations were run until 2% statistical uncertainty on doses in the volumes of interest was reached. In general, the most

efficient simulations are those with tracklength scoring and employing a phase-space source; the simulation times quoted in this paragraph are for these calculations. Times in parentheses in the next sentence indicate the total time, including initialization of the simulation and geometry, outputting results, etc. Simulations achieving 2% statistical uncertainty in the prostate with $(2\,\text{mm})^3$ voxels ('i') take 10 s (13 s); $(1\,\text{mm})^3$ voxels ('h') take 57 s (63 s). Simulations of the eye plaque in a water phantom with $(1\,\text{mm})^3$ voxels ('m') take less than 15 s (22 s) to achieve 2% uncertainty; with a more detailed phantom with smaller voxels ('l'), simulations take at most 79 s (95 s). For breast ^{103}Pd calculations ('o'), 2% uncertainty in $(2\,\text{mm})^3$ voxels comprising the PTV take less than 35 s (39 s); similarly for breast ^{192}Ir calculations ('o'), 2% uncertainty is reached in 147 s (151 s).

Some of the individual features used to enhance egs_brachy simulation efficiency have been employed in other MC brachytherapy-specific codes. In their photon-specific code for prostate implants, MCPI, Chibani and Williamson (2005) employed a tracklength estimator for scoring dose and phase-space data as source of initial particles in simulations, in addition to geometric considerations (discretizing internal seed structure, simplified seed models rather full source geometry modelling, voxel-indexing of seeds). They employed ray tracing to enhance MCPI efficiency rather than using analog photon transport (Chibani and Williamson 2005)—the latter is employed in egs_brachy. In the PTRAN code (Williamson 1987, Li and Williamson 1992), use of a tracklength estimator over interaction scoring results in 10 to 100-fold increase in efficiency (Hedtjärn *et al* 2002), similar to results obtained with egs_brachy. Afsharpour *et al* (2012) also reported on a brachytherapy-specific Geant4-based MC code, ALGEBRA, which employs a phase-space source and tracklength estimator to score collision kerma; however, efficiency gains or time reductions due to these features are not reported. Characterization of efficiency gains is highly dependent on both the code in which the features are implemented and the code used for comparison.

The present characterization of features to enhance efficiency has been done within the same code by comparing efficiencies for simulations with and without the features. This performance assessment generalizes beyond any one code. With the development and adoption of MBDCA for brachytherapy, other codes may benefit from the techniques presented herein to assess calculation efficiency. For example, other codes may use the same idealized configurations used in this study (prostate and breast permanent implants, eye plaque, etc) to conduct speed benchmarks.

3.2.3. Electronic brachytherapy. Finally, consider the 50 kV electronic brachytherapy configuration ('c'). Using a phase-space source, the efficiency is $5.0 \times 10^{-3}\,\text{s}^{-1}$, which is comparable to the efficiencies reported for radionuclide sources in table 6. The efficiency gain factor is 1.11×10^4 over the *ab initio* simulation, which indicates simulation of radiation transport within the source is very time-consuming. The simulation with electrons initialized within the source but with BCSE ($f_{\text{enh}} = 500$) and UBS ($N_{\text{split}} = 100$) is 2.1×10^3 times more efficient than the *ab initio* analog simulation, but still an order of magnitude less efficient than using a phase-space source (ignoring the time to calculate the phase-space file). An *ab initio* simulation of the x-ray source takes up to 153 h to achieve 2% uncertainty on doses to the $(1\,\text{mm})^3$ voxels in the $(2\,\text{cm})^3$ cube, whereas simulations with the phase-space source take 50 s and those with BCSE and UBS take 4.5 min. Efficiency gains of range rejection are negligible for this particular configuration. Although the efficiency gains of using BCSE and UBS are smaller than using a phase-space source, the usefulness of the variance reduction techniques should not be underestimated for research and development purposes (for example, when fine-tuning new x-ray source parameters to match experimental measurements). The ability

Table 7. Times to reach specified uncertainties in different volumes of interest ('Metric') for example clinical cases.Both simulation times (CPU time spent on radiation transport) and total times (from when egs_brachy is launched to when it exits) are also reported. Configurations are described in table 2.

Treatment	Radio-nuclide	# seeds	Configuration	Simulation time (s)	Total time (s)	Metric
Breast LDR	^{103}Pd	49	'p'	38	48	2%—PTV
				23	34	5%—Skin
Breast HDR	^{192}Ir	79[a]	'q'	102	119	2%—PTV
				222	238	5%—Skin
Prostate LDR	^{125}I	67	'r'	29	38	2%—PTV
				21	30	5%—Bladder
				15	22	5%—Rectum
				7	16	5%—Urethra

[a] Number of dwell positions.

to model electron sources such as miniature x-ray tube and beta emitting eye plaques is a strength of the egs_brachy code system compared to photon-specific brachytherapy codes.

3.3. Calculation times for clinical configurations

Table 7 shows calculation times for the three clinical configurations considered ('p', 'q', 'r'). Most total times when egs_brachy is run on one processor core are below 1 min, which includes the time for simulation and geometry initialization, outputting and combining results, etc. The breast HDR treatment takes 4 min to reach 5% uncertainty on doses to the skin. The time for initializing the simulation and the geometry and for outputting results depends on factors such as disk read and write speeds, CPU speed, number of voxels and media in the geometry, etc. Shorter simulation times can be achieved by running calculations in parallel. Note that times will vary with patient and treatment (location and number of seeds, radionuclide, volumes of PTV and organs at risk, proximity of organs at risk to sources, etc).

egs_brachy calculation times are comparable or faster to those achievable with other brachytherapy-specific Monte Carlo codes on CPUs (Chibani and Williamson 2005, Afsharpour *et al* 2012, Chibani and Ma 2014). However, calculation times depend on CPU used, so a direct comparison to other codes is meaningless unless performed on similar hardware. We note that egs_brachy is comparable in speed or faster than BrachyDose (Taylor *et al* 2007, Thomson *et al* 2010), but timing results were never comprehensively reported in the literature for the latter.

4. Conclusions

egs_brachy dose distributions agree with BrachyDose on a sub-percent level. TG-43 parameters calculated with egs_brachy also agree within uncertainties with published values. For photon sources, it is found that the largest gain in simulation efficiency comes from using a tracklength estimator to score collision kerma (factor of 10 to 300 over interaction scoring). The `EGS_AutoEnvelope` geometry class for simulations including multiple

seeds and small voxels improves efficiency by a factor of up to 4.6 for 100 seeds in $(1\,\text{mm})^3$ voxels. Use of a phase-space source or of particle recycling can further increase the efficiency by a factor of 2. For electronic brachytherapy, the efficiency is improved by more than four orders of magnitude with the use of a phase-space source. BCSE and UBS variance reduction techniques increase the efficiency by a factor of 2.1×10^3 over *ab initio* simulations. Resulting egs_brachy calculation times for realistic LDR clinical scenarios are below 1 min using a single processor core (below 4 min for HDR). As the brachytherapy community moves towards greater clinical adoption of model-based dose calculations for brachytherapy, it is the authors' hope that egs_brachy will contribute to advancing dosimetry. To that end, egs_brachy will be released as free and open source software to the scientific community for research purposes. (see http://physics.carleton.ca/clrp/egs_brachy)

Acknowledgments

This work was supported by the Natural Sciences and Engineering Research Council of Canada, the Canada Research Chairs program, and the Ministry of Research and Innovation of Ontario. The authors thank Compute/Calcul Canada and the Shared Hierarchical Academic Research Computing Network (SHARCNET) for access to computing resources, Justin Sutherland and Marielle Lespérance for providing the breast and eye egsphant files, respectively; Stephen Deering for the eye plaque model and for general egs_brachy testing during his research; and Joanna Cygler from The Ottawa Hospital Cancer Centre for the breast and prostate LDR clinical plans.

References

Afsharpour H, Landry G, D'Amours M, Enger S, Reniers B, Poon E, Carrier J F, Verhaegen F and Beaulieu L 2012 ALGEBRA: Algorithm for the heterogeneous dosimetry based on GEANT4 for BRAchytherapy *Phys. Med. Biol.* **57** 3273–80

Ali E S M and Rogers D W O 2007 Efficiency improvements of x-ray simulations in EGSnrc user-codes using bremsstrahlung cross section enhancement (BCSE) *Med. Phys.* **34** 2143–54

Ballester F *et al* 2015 A generic high-dose rate ^{192}Ir brachytherapy source for evaluation of model-based dose calculations beyond the TG-43 formalism *Med. Phys.* **42** 3048–62

Beaulieu L, Tedgren A C, Carrier J F, Davis S D, Mourtada F, Rivard M J, Thomson R M, Verhaegen F, Wareing T A and Williamson J F 2012 Report of the Task Group 186 on model-based dose calculation methods in brachytherapy beyond the TG-43 formalism: current status and recommendations for clinical implementation *Med. Phys.* **39** 6208–36

Berger M J and Hubbell J H 1987 XCOM: photon cross sections on a personal computer *Report* NBSIR87–3597 (Gaithersburg, MD: National Institute of Standards Technology (NIST))

BIPM 2011 Monographie BIPM-5: Table of Radionuclides: vol 6 *Technical Report* (Sevres: BIPM) (www.bipm.org/en/publications/scientific-output/monographie-ri-5.html)

Bonenfant E, Magnoux V, Hissoiny S, Ozell B, Beaulieu L and Despes P 2015 Fast GPU-based Monte Carlo simulations for LDR prostate brachytherapy *Phys. Med. Biol.* **60** 4973–86

Brookhaven National Laboratory, National Nuclear Data Center www.nndc.bnl.gov/nudat2

Chibani O and Ma C M C 2014 HDRMC, an accelerated Monte Carlo dose calculator for high dose rate brachytherapy with CT-compatible applicators *Med. Phys.* **41** 051712

Chibani O and Williamson J F 2005 MCPI: a sub-minute Monte Carlo dose calculation engine for prostate implants *Med. Phys.* **32** 3688–98

Hedtjärn H, Carlsson G A and Williamson J F 2002 Accelerated Monte Carlo based dose calculations for brachytherapy planning using correlated sampling *Phys. Med. Biol.* **47** 351–76

Kawrakow I and Fippel M 2000 Investigation of variance reduction techniques for Monte Carlo photon dose calculation using XVMC *Phys. Med. Biol.* **45** 2163–84

Kawrakow I, Mainegra-Hing E, Rogers D W O, Tessier F and Walters B R B 2011 The EGSnrc code system: Monte Carlo simulation of electron and photon transport NRC *Technical Report* PIRS-701 v4-2-3-2 (Ottawa: National Research Council Canada) (www.nrc-cnrc.gc.ca/eng/solutions/advisory/egsnrc/download_egsnrc.html)

Kawrakow I, Mainegra-Hing E, Tessier F and Walters B R B 2009 The EGSnrc C++ class library *Technical Report* PIRS-898 (rev A) (Ottawa: National Research Council Canada) (www.irs.inms.nrc.ca/EGSnrc/PIRS898/)

Kennedy R M, Davis S D, Micka J A and DeWerd L A 2010 Experimental and Monte Carlo determination of the TG-43 dosimetric parameters for the model 9011 THINSeed brachytherapy source *Med. Phys.* **37** 1681–8

Lesperance M, Inglis-Whalen M and Thomson R M 2014 Model-based dose calculations for COMS eye plaque brachytherapy using an anatomically realistic eye phantom *Med. Phys.* **41** 021717

Li Z and Williamson J F 1992 Volume-based geometric modeling for radiation transport calculations *Med. Phys.* **19** 667–77

Miksys N, Cygler J E, Caudrelier J M and Thomson R M 2016a Patient-specific Monte Carlo dose calculations for ^{103}Pd breast brachytherapy *Phys. Med. Biol.* **61** 2705–29

Miksys N, Vigneault E, Martin A G, Beaulieu L and Thomson R M 2016b Large scale retrospective Monte Carlo dosimetric study for permanent implant prostate brachytherapy *Intl J. Rad. Biol. Phys.* submitted

Nath R, Yue N, Shahnazi K and Bongiorini P 2000 Measurement of dose-rate constant for ^{103}Pd seeds with air kerma strength calibration based upon a primary national standard *Med. Phys.* **27** 655–8

NCRP Report 58 1985 *A Handbook of Radioactivity Measurements Procedures* (Bethesda, MD: NCRP Publications)

Papagiannis P, Pantelis E and Karaiskos P 2014 Current state of the art brachytherapy treatment planning dosimetry algorithms *Br. J. Radiol.* **87** 20140163

Peppa V, Pantelis E, Pappas E, Lahanas V, Loukas C and Papagiannis P 2016 A user-oriented procedure for the commissioning and quality assurance testing of treatment planning system dosimetry in high-dose-rate brachytherapy *Brachytherapy* **15** 252–62

Perkins S T, Cullen D E, Chen M H, Hubbell J H, Rathkopf J A and Scofield J H 1991 *Tables and Graphs of Atomic Subshell and Relaxation Data Derived from the LLNL Evaluated Atomic Data Library (EADL), Z = 1–100* (*Lawrence Livermore National Laboratory Report UCRL-50400* vol 30) (Livermore, CA: Lawrence Livermore National Laboratory)

Rivard M J, Coursey B M, DeWerd L A, Huq M S, Ibbott G S, Mitch M G, Nath R and Williamson J F 2004 Update of AAPM Task Group No. 43 report: a revised AAPM protocol for brachytherapy dose calculations *Med. Phys.* **31** 633–74

Rivard M J *et al* 2011 Comparison of dose calculation methods for brachytherapy of intraocular tumors *Med. Phys.* **38** 306–16

Rodriguez M and Rogers D W O 2013 On determining dose rate constants spectroscopically *Med. Phys.* **40** 011713

Rodriguez M and Rogers D W O 2014 Effect of improved TLD dosimetry on the determination of dose rate constants for ^{125}I and ^{103}Pd brachytherapy seeds *Med. Phys.* **41** 114301

Russell K R, Carlsson-Tedgren A K and Ahnesjö A 2005 Brachytherapy source characterization for improved dose calculations using primary and scatter dose separation *Med. Phys.* **32** 2739–52

Sutherland J G H, Thomson R M and Rogers D W O 2011 Changes in dose with segmentation of breast tissues in Monte Carlo calculations for low-energy brachytherapy *Med. Phys.* **38** 4858–65

Taylor R E P and Rogers D W O 2008a An EGSnrc Monte Carlo-calculated database of TG-43 parameters *Med. Phys.* **35** 4228–41

Taylor R E P and Rogers D W O 2008b EGSnrc Monte Carlo calculated dosimetry parameters for ^{192}Ir and ^{169}Yb brachytherapy sources *Med. Phys.* **35** 4933–44

Taylor R E P, Yegin G and Rogers D W O 2006 Monte Carlo modeling of the Xoft Axxent x-ray source *Med. Phys.* **33** 2205

Taylor R E P, Yegin G and Rogers D W O 2007 Benchmarking BrachyDose: voxel-based EGSnrc Monte Carlo calculations of TG-43 dosimetry parameters *Med. Phys.* **34** 445–57

Thomadsen B R, Williamson J F, Rivard M J and Meigooni A S 2008 Anniversary paper: past and current issues, and trends in brachytherapy physics *Med. Phys.* **35** 4708–20

Thomson R M, Taylor R E P and Rogers D W O 2008 Monte Carlo dosimetry for ^{125}I and ^{103}Pd eye plaque brachytherapy *Med. Phys.* **35** 5530–43

Thomson R M, Yegin G, Taylor R E P, Sutherland J G H and Rogers D W O 2010 Fast Monte Carlo dose calculations for brachytherapy with BrachyDose *Med. Phys.* **37** 3910–1

Walters B R B, Kawrakow I and Rogers D W O 2002 History by history statistical estimators in the BEAM code system *Med. Phys.* **29** 2745–52

Williamson J F 1987 Monte Carlo evaluation of kerma at a point for photon transport problems *Med. Phys.* **14** 567–76

Woodard H Q and White D R 1986 The composition of body tissues *Br. J. Radiol.* **59** 1209–19

Yegin G 2003 A new approach to geometry modelling of Monte Carlo particle transport: an application to EGS *Nucl. Instrum. Methods* B **211** 331–8